JOURNAL OF SOLID STATE CHEMISTRY 70, 249–261 (1987)

The Magnetic Phase Diagram of $HoGe_{1-x}Si_x$ Studied by Neutron Diffraction and Magnetic Measurements*

P. SCHOBINGER-PAPAMANTELLOS†

Institut für Kristallographie und Petrographie ETHZ, CH-8092 Zurich, Switzerland

AND K. H. J. BUSCHOW

Philips Research Laboratories, 5600 JA Eindhoven, The Netherlands

Received December 18, 1986

Several samples ($0.2 \leq x \leq 1.0$) of $HoGe_{1-x}Si_x$ (CrB type) were studied over an extensive temperature range by neutron diffraction. The relative stability of the two existing magnetic structures with wave vectors $[\frac{1}{2}\ 0\ \frac{1}{2}]$ and $[q_x\ 0\ q_z]$ depends on both the temperature and composition. The corresponding stability regions are shown in a magnetic phase diagram. The Néel temperature T_N and the transition temperature T_{ic} between the lock-in structure and the incommensurate structure increase with silicon content. At T_{ic} the wave vector jumps from the $[\frac{1}{2}\ 0\ \frac{1}{2}]$ value to the incommensurate value $[q_x\ 0\ q_z]$. With increasing temperature the q_x and q_z components show a linear decrease and increase, respectively. The transition at T_{ic} is most probably of first order. The magnetic moments of Ho are confined to a direction close to the c-axis (5–7°) over the whole temperature range and order with a pure sinus modulation between T_{ic} and T_N. © 1987 Academic Press, Inc.

1. Introduction

The end members of the pseudobinary system $HoGe_{1-x}Si_x$ crystallize with the CrB type of structure ($x = 0$), or with both the CrB and FeB types ($x = 1$) (*1*). The CrB type considered in the course of the present study has the orthorhombic space group $Cmcm(D_{2h}^{17})$. All atoms occupy the low symmetry position 4(c) with the atomic position parameters $y_{Ho} = 0.14$ and $y_{Ge,Si} = 0.42$. The magnetic properties show predominantly an antiferromagnetic behavior. The Néel temperatures are equal to $T_N = 18$ K for HoGe (*2*) and $T_N = 25$ K for HoSi (*3*). In a previous neutron investigation (*4*) it was shown experimentally that the magnetic structure of HoGe remains incommensurate with the crystal lattice over the whole temperature range from 1.2 K to $T_N = 18$ K, while HoSi was reported to order with a commensurate structure with the wave vector $k = [\frac{1}{2}\ 0\ \frac{1}{2}]$, in which the moments were close (16°) to the c-axis. The same structure resulted from the 4.2 K data of HoGe if one neglects the slight deviation from the lock-in value $[\frac{1}{2}\ 0\ \frac{1}{2}]$. The wave vector of the incommensurate structure was approximated at 4.2 K to the value [0.506, 0., 0.506]. Although we recognized that the

* Dedicated to Dr. H. Nowotny.

† Permanent guest scientist at the Laboratorium für Neutronenstreuung, ETHZ, CH-5303 Würenlingen.

0022-4596/87 $3.00

Copyright © 1987 by Academic Press, Inc.
All rights of reproduction in any form reserved.

wave vector was incommensurate in two directions q_x and q_z we have not been able to give a complete interpretation of the data of the incommensurate structure. The main difficulties arose from the presence of impurities and from the absence of sufficient experimental information regarding the plane containing the wave vector $(h0l)$ which is necessary for deriving the exact q_x and q_z values.

On the other hand, in a recent investigation of $TbGe_{1-x}Si_x$ compounds (*5*), which show a similar modulated structure, the use of difference diagrams based on neutron data obtained for the ordered and the paramagnetic state has proved to be quite helpful. In fact, it follows from the successful data analysis made for these materials that this technique makes it possible to obtain approximate values of the wave vector components and follow their evolution over the whole temperature range. The application of this technique opens the possibility to reinvestigate the incommensurate structure of HoGe by obtaining more complete neutron data using the DMC (double-axis multicounter system, see next section) and construct the necessary difference diagrams. Owing to the relevance of the information that can be obtained by difference diagrams it seems interesting to extend this investigation over the whole system $HoGe_{1-x}Si_x$ and study the change in wave vectors as a function of concentration.

It will be shown that the incommensurate structure is restricted only to a high-temperature region $T_{ic} \leq T \leq T_N$ for $x > 0.2$ and that there is a linear increase of T_{ic} (incommensurate to commensurate transition temperature) and of T_N with silicon content. These results are used for constructing a (T, x) magnetic phase diagram.

2. Experimental Procedure and Results

The powder samples of $HoGe_{1-x}Si_x$ ($0.2 \leq x \leq 1.0$) used in the present investigation were prepared by means of arc-melting in an atmosphere of purified argon gas. The purity of the starting materials was 99.9% for Ho and 99.99% for Ge and Si. X-ray diffraction showed that up to $x = 0.9$ all samples have single phase (CrB-type) X-ray diagrams composed of sharp reflections, the width of which did not change upon alloying. Thus the $HoGe_{1-x}Si_x$ system behaves as a normal solid solution system and its lattice constants follow a linear decrease between the end members HoGe and HoSi. The latter compound was found to crystallize with both the CrB and FeB structure types.

2.1. Neutron Diffraction and Magnetic Measurements

The neutron diffraction data in the temperature range 1.2 to 293 K were collected with the DMC system, ($\lambda = 2.323$ Å and in some cases 1.709 Å) at the Saphir reactor (Würenlingen). The step increment of the diffraction angle 2θ was 0.10°. The DMC system is suitable to study phase transitions since it allows the collection of experimental information over a 2θ region of 80° simultaneously. The data were corrected for absorption and evaluated by the line profile analysis method for all nuclear and commensurate magnetic structures (*6*); a special program based on integrated intensities was used for the intensity calculation of the incommensurate phases.

Magnetic measurements on all samples examined were made in the temperature range 4.2 to 600 K. The values of T_N, θ_p, and experimental μ_{eff} of all these materials are listed in Table I and compared to the values resulting from the neutron data. The μ_{eff} value corresponds to the free ion value of Ho^{3+}. The Néel temperature was found to increase linearly with silicon content, which is in good agreement with the neutron results.

As will be be discussed in more detail in the next section, the $HoGe_{1-x}Si_x$ system for

TABLE I

MAGNETIC PROPERTIES OF THE $HoGe_{1-x}Si_x$ COMPOUNDS AS STUDIED BY MAGNETIC MEASUREMENTS AND NEUTRON DIFFRACTION

	Magnetic measurements			Neutron diffraction	
x	T_N(K)	θ_p(K)	$\mu_{eff}(\mu_B/Ho)$	T_N(K)	T_{ic}(K) (heating)
0.0	18	−5	10.77	18.0 ± 0.5	<1.2
0.2	20	−5	10.82	19.0 ± 0.5	<1.2
0.3	20	−2	10.76	19.7 ± 0.5	10.5 ± 5
0.5	22	−2	10.80	21.5 ± 0.5	12.5 ± 0.5
0.8	24	0	10.79	23.0 ± 0.5	15.5 ± 0.5
1.0	25	2	10.64	25.5 ± 0.5	19.0 ± 0.5

Note. T_N and θ_p are the Néel temperatures and asymptotic Curie temperatures, respectively. T_{ic} is the temperature of the commensurate to incommensurate phase transition. The effective moments from magnetic measurements are represented by μ_{eff}.

$x > 0.2$ was found to order with a commensurate phase having the wave vector $[\frac{1}{2}\ 0\ \frac{1}{2}]$ at low temperatures and with a structure modulated in two dimensions and having a wave vector $[q_x\ 0\ q_z]$ in the high-temperature region. Since the nuclear structure and the commensurate magnetic structure observed in this system have been described before (*3*, *4*), we restrict ourselves to summarize all refined parameters of the corresponding neutron diagrams. These are listed in Table II for comparison. The refinement of the 293 K nuclear structures is based on neutron data obtained with a wavelength equal to $\lambda = 1.709$ Å, which made it possible to get a relatively large amount of information. The temperature-dependent measurements were performed using $\lambda = 2.323$ Å, which had the advantage of reducing the measuring time by a factor of 4. Examples of refined profiles are given in Figs. 1 and 2. The scattering lengths used in the refinements were taken from Ref. (*7*) and the magnetic form factor for Ho^{3+} was taken from Ref. (*8*).

The refined lattice constants at 293 K given for all compounds in Table II show a linear decrease with silicon content. The lattice constants of (CrB-type) HoSi, which were not refined in the present study (mixture of CrB and FeB), are equal to $a = 4.228$, $b = 10.429$, and $c = 3.801$ Å (*1*). The largest decrease in the lattice constants was observed in the c direction and the second largest decrease was in the b direction. The values of a were found to be almost independent of silicon content. Similar behavior was found in the $TbGe_{1-x}Si_x$ system (*5*). The refinement of the (Ge, Si) occupancy parameters did not have any influence on

TABLE II

THE REFINED PARAMETERS FROM THE 293 AND 4.2 K NEUTRON DATA FOR $HoGe_{1-x}Si_x$ (x = 0., 0.2, 0.5, AND 0.8) FOR THE NUCLEAR AND THE COMMENSURATE MAGNETIC STRUCTURE

	293 K				4.2 K	
Parameter	HoGe	$HoGe_{0.8}Si_{0.2}$	$HoGe_{0.5}Si_{0.5}$	$HoGe_{0.2}Si_{0.8}$	$HoGe_{0.5}Si_{0.5}$	$HoGe_{0.2}Si_{0.8}$
a (Å)	4.2428(9)	4.2362(3)	4.2347(4)	4.2306(3)	8.466(1)	8.448(1)
b (Å)	10.623(3)	10.574(1)	10.520(1)	10.472(1)	10.493(1)	10.436(1)
c (Å)	3.919(1)	3.8915(3)	3.8566(3)	3.825(1)	7.681(1)	7.617(1)
y_{Ho}	0.1381(6)	0.1391(3)	0.1401(3)	0.1404(3)	0.1411(8)	0.1418(6)
$y_{Ge,Si}$	0.4168(6)	0.4158(3)	0.4182(4)	0.4207(4)	0.4184(7)	0.4203(9)
B_{ov} (Å)^2	0.6(1)	0.18(6)	0.11(8)	0.25(3)	0.47(3)	0.33(6)
$\mu(\mu_B)$, θ_z(°)	—	—	—	—	7.9(5),8(2)	7.90(6),7(1)
R_n (%)	12	7.2	7.5	6.5	8.5	8
R_m (%)	—	—	—	—	6.3	6.4
R_{wp} (%)	16	11.3	13.2	11.5	11.8	13
R_{exp} (%)	6.5	4.1	7	4.9	2.1	4.6

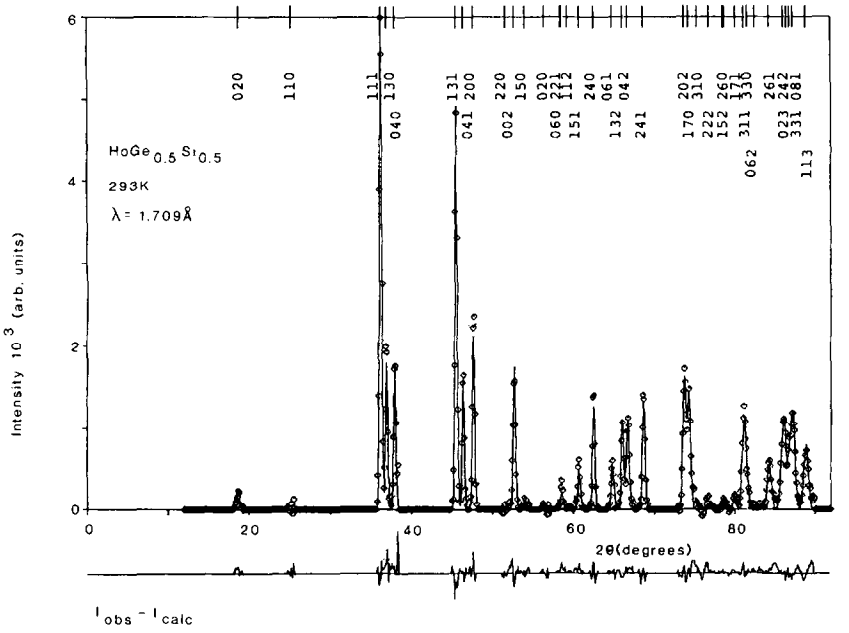

FIG. 1. Neutron diffraction pattern of $HoGe_{0.5}Si_{0.5}$ at 293 K. The full curve represents the calculated profiles; the data points represent the observed intensities. The difference diagram is indicated at the bottom of the figure.

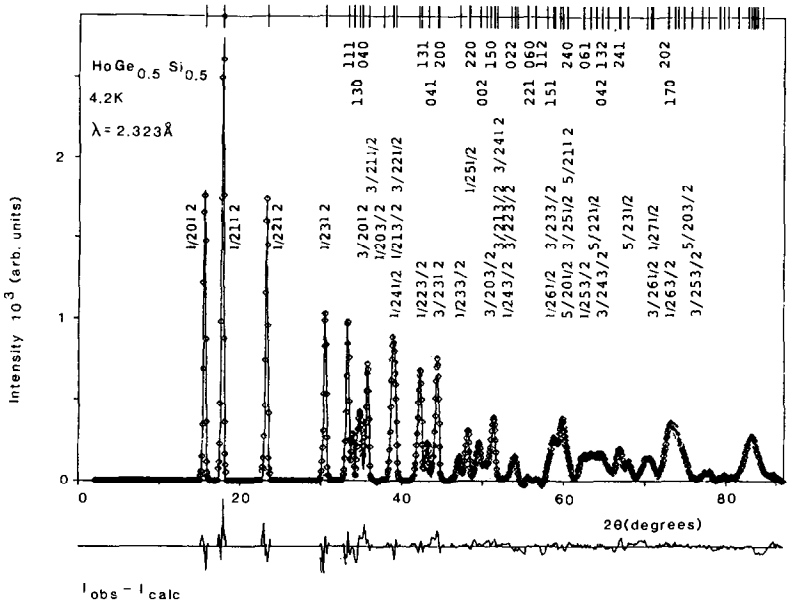

FIG. 2. Neutron diffraction pattern of $HoGe_{0.5}Si_{0.5}$ at 4.2 K. The full curve represents the calculated profiles; the data points represent the observed intensities. The difference diagram is indicated at the bottom of the figure.

the R factors. For samples containing Si, a lower R value is found than for pure HoGe (*4*), since alloying with Si was found to suppress the amount of foreign phases observed in this latter sample to a large extent. From the fact that the overall temperature factors are somehow rather low we may assume that some impurity lines overlapping with the reflections of the main phase might still be present.

The commensurate magnetic structures of the $HoGe_{0.5}Si_{0.5}$ and $HoGe_{0.2}Si_{0.8}$ compounds associated with the wave vector $[\frac{1}{2}\ 0\ \frac{1}{2}]$ are refined from the 4.2 K data. It can be seen in Table II that the two structures have the same moment value for Ho, 7.90 μ_B, and the same moment direction, 7(1)°, relative to the c-axis and are located in the (x 0 z) plane. These values are slightly different from the data reported for HoSi (*3*) where the magnetic moment was found to be parallel to the $[\bar{1}03]$ direction. In Ref. (*5*) a canted model has been proposed for this structure (occurring also in the $TbGe_{1-x}Si_x$ system), instead of the collinear structure proposed in Refs. (*3*, *7*). The same arguments discussed extensively in Ref. (*5*) are valid for the $HoGe_{1-x}Si_x$ system. The canted model gives the same magnetic intensities as the collinear model but it has a twofold axis in addition to the B_a magnetic lattice of the collinear model. The magnetic space group is B_a2 (Sh_5^{17}) (*5*, *9*). The two structures are compared in Fig. 8.

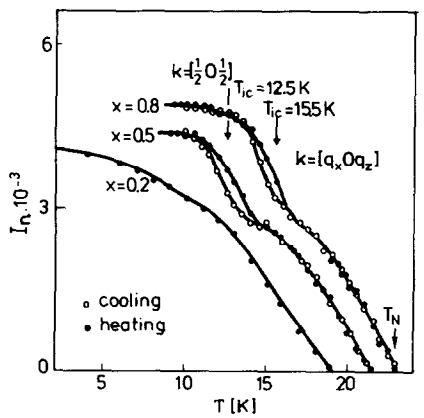

FIG. 3. Temperature dependence of the magnetic intensity of the zero-point satellite observed upon cooling and heating in three compounds of the Ho $Ge_{1-x}Si_x$ system.

The compound $HoGe_{0.8}Si_{0.2}$, like the compound HoGe, remains incommensurate (see next section) over the whole temperature range extending from 1.2 K to T_N = 19 K and is therefore not included in Table II.

All refined magnetic structures show a satisfactory agreement between observed and calculated data which is reflected in the low values of the magnetic reliability factors of 6.3%.

2.2. *The Temperature Dependence of Magnetic Intensities*

For the temperature-dependent measurements we used a liquid helium cryostat with variable temperature for all the samples up to the composition x = 0.5, and a closed-cycle He refrigerator for the other samples. The changes of the magnetic intensity were observed for a large number of magnetic peaks up to the 2θ value of 83°.

In order to follow the commensurate to incommensurate phase transition, the first five resolved magnetic peaks (see Fig. 2) were evaluated by using a multi-Gauss fitting procedure which provided the integrated intensities, the half-widths, and the 2θ positions. Representative results are shown in Fig. 3 for the reflection $[\frac{1}{2}\ 0\ \frac{1}{2}]$ located at 2θ = 23.4° and in Fig. 5 for the reflection $[\frac{1}{2}\ 1\ \frac{1}{2}]$ located at 2θ = 26.8°. The former reflection is the zero-point satellite of the magnetic cell and is therefore a single peak. It may be seen that the intensity for the compound with x = 0.2 changes continuously in the whole temperature range extending from 1.2 K to T_N while the 2θ moves to smaller angles. This compound behaves like HoGe where the lock-in structure may occur below 1.2 K.

By contrast, the two compounds Ho

$Ge_{0.5}Si_{0.5}$ and $HoGe_{0.2}Si_{0.8}$ are commensurate in the low-temperature region extending from 1.2 K to T_{ic}. The magnetic intensity of the zero-point satellite is changing discontinuously at the transition from the commensurate to the incommensurate structure and the peak position shows a small shift to lower angles. As will be shown in the next section the wave vector jumps to the incommensurate value when heating to above T_{ic}.

This jump, however, is not visible from the line shift of the zero-point satellite (Table III) because the q_x and the q_z components of the wave vector change in different directions [0.45, 0., 0.511].

The incommensurate to commensurate transition is most probably a first-order transition. It may be seen from Fig. 3 that a small hysteresis (1 ± 0.25 K) has been observed upon cooling or heating the two compounds with $x = 0.5$ and $x = 0.8$. From the increase in half-width of the zero-point satellite within a given temperature region, as shown in Fig. 4, it can be concluded that a region of coexistence exists between the lock-in structure and the incommensurate structure. This is rather common for first-order phase transitions. The transition temperature T_{ic} corresponds to a temperature located in the middle of the region where the two structure types are found to coexist when heating the sample. The dependence

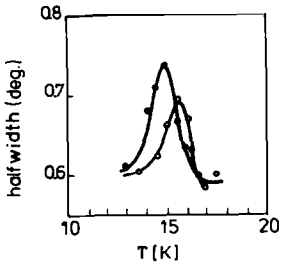

FIG. 4. The change in half-width of the zero-point satellite. [½ 0 ½] in the transition region during cooling (full symbols) and heating of the compound Ho $Ge_{0.2}Si_{0.8}$ (open symbols).

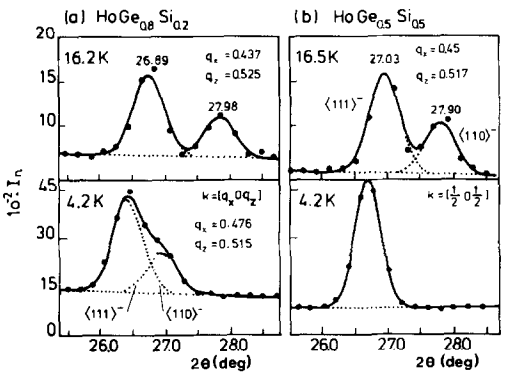

FIG. 5. The splitting of the [½ 1 ½] magnetic peak for the same temperatures and the same compounds as considered in Fig. 3.

of the incommensurate to commensurate transition on both the temperature and concentration is better illustrated in Fig. 5, where the behavior of the [½ 1 ½] satellite for the compounds $HoGe_{0.8}Si_{0.2}$ and $HoGe_{0.5}Si_{0.5}$ at 4.2 and 16 K is shown. At 4.2 K the [½ 1 ½] peak is a single reflection for $HoGe_{0.5}Si_{0.5}$, but consists of two magnetic satellites for $HoGe_{0.8}Si_{0.2}$ (111^-, 110^-) which move to higher angles and continue to diverge with increasing temperature. At 16.5 K the splitting of this satellite is 1.1° for $x = 0.2$ and 0.8° for $x = 0.5$. As will be shown in the next section the splitting of this satellite depends exclusively on the q_z wave vector component. The values of T_{ic} together with those of T_N are summarized in Table I. The 16.5 K data of $HoGe_{0.2}Si_{0.8}$ have been used for determining the structure of the incommensurate phase.

2.3. *The Incommensurate Structure of* $HoGe_{1-x}Si_x$ ($T_{ic} \leq T \leq T_N$)

The indexing of the magnetic reflections of the incommensurate phase was made by means of the formula (4)

$$d^{*2} = \frac{4 \sin^2\theta}{\lambda^2} = (h \pm q_x)^2 a^{*2} + k^2 b^{*2} + (l \pm q_z)^2 c^{*2}. \quad (1)$$

TABLE III

OBSERVED AND CALCULATED INTEGRATED MAGNETIC NEUTRON INTENSITIES OF $HoGe_{0.2}Si_{0.8}$

4.2 K ($\mathbf{k}$ = [½ 0 ½])						16 K ($\mathbf{k}$ = [0.459, 0, 0.511])						
h	k	l	$2\theta_{calc}$	I_{obs}	I_{calc}	h	k	l	$2\theta_{calc}$	$2\theta_{obs}$	I_{obs}	I_{calc}
½	0	½	23.48	4762	4721	0	0	0^+	23.05	23.15	2075	2027
½	1	½	26.79	8004	7491	1	1	1^-	27.47	27.45	3622	3528
						1	1	0^-	27.98	27.96		
½	2	½	35.04	4893	5021	0	2	1^-	34.46	34.46	2678	2568
						0	2	0^+	34.78			
½	3	½	45.93	3164	3415	1	3	1^-	46.41	46.60	1783	1552
						1	3	0^-	46.74			
⅔	1	½	53.73	3000	2557	1	1	$\bar{1}^+$	52.40	52.69	1499	1244
						1	1	0^+	52.70			
⅔	0	½	51.95	1216	1252	2	0	0^-	53.59	53.56	615	581
½	0	⅔	56.85	0	35	0	0	2^-	56.15			
½	4	½	58.49	2331	2289	0	4	1^-	58.09	58.37	1211	1035
						0	4	0^+	58.36			
½	1	⅔	58.52	325	321	1	1	$\underline{2}^-$	58.67			
						1	1	$\bar{1}^-$	59.49			
⅔	2	½	58.84	2338	2349	2	2	1^-	60.08	59.95	1287	1158
						2	2	0^-	60.35			
½	2	⅔	63.38	619	654	0	2	2^-	62.74	63.60	401	260
						0	2	1^+	63.53			
⅔	3	½	66.81	1937	1795	1	3	$\bar{1}^+$	65.66	65.95	1023	812
						1	3	0^-	65.92			
½	3	⅔	71.07	706	705	1	3	$\underline{2}^-$	71.22	71.29	484	303
						1	3	$\bar{1}^-$	71.96			
½	5	½	72.54	1577	1524	1	$\bar{5}$	1^-	72.94	72.87	815	654
						1	5	0^-	73.18			
⅔	1	⅔	77.28	746	700	1	1	$\bar{2}^+$	75.97	76.63	400	300
						1	1	1^-	76.69			
⅔	0	⅔	75.82	501	425	2	0	2^-	76.70			
⅔	4	½	77.25	1372	1291	2	4	1^-	78.37	78.33	515	539
						2	4	0^-	78.61			
½	4	⅔	81.32	638	635	0	4	2^-	80.74	80.69	278	275
						0	4	1^+	81.45			
⅔	2	⅔	81.61	531	529	2	2	$\underline{2}^-$	82.47	83.10	275	234
						2	2	$\bar{1}^-$	83.18			
⅔	0	½	89.30	549	543	2	0	0^+	87.78			
⅔	3	⅔	88.73	588	573	1	3	$\bar{2}^+$	87.46			
						1	3	1^+	88.16	88.16	1542	1124
½	6	½	88.41	1104	1057	0	6	1^-	88.09			
						0	6	0^+	88.32			
⅔	5	½	90.13	1001	994	1	5	$\bar{1}^+$	89.09			
						1	5	0^+	89.32			
⅔	1	½	90.72	1070	1014	3	1	1^-	92.52	92.89	1042	787
						3	1	0^-	92.76			
⅔	2	½	94.98	928	893	2	2	$\bar{1}^+$	93.23			
						2	2	0^+	93.46			
½	5	⅔	94.12	598	595	1	5	$\underline{2}^-$	94.27			300
						1	5	$\bar{1}^+$	94.97			
⅔	4	⅔	98.70	558	651	2	4	$\underline{2}^-$	99.57			255
						2	4	$\bar{1}^-$	100.29			

Note. *hkl* are the magnetic satellites referring to the *a*, *b*, *c* cell.

All observed magnetic satellites (Fig. 6) of the neutron data of $HoGe_{0.2}Si_{0.8}$ obtained at 16 K (referring to the chemical C-cell) were calculated with the refined wave vector value [0.459, 0., 0.511] (see next section). From recent intensity calculations (*5b*, *10*) it has been found that the modulated magnetic structure corresponds to a pure two-dimensional sinus modulation and not to a spiral model as suggested previously (*4*).

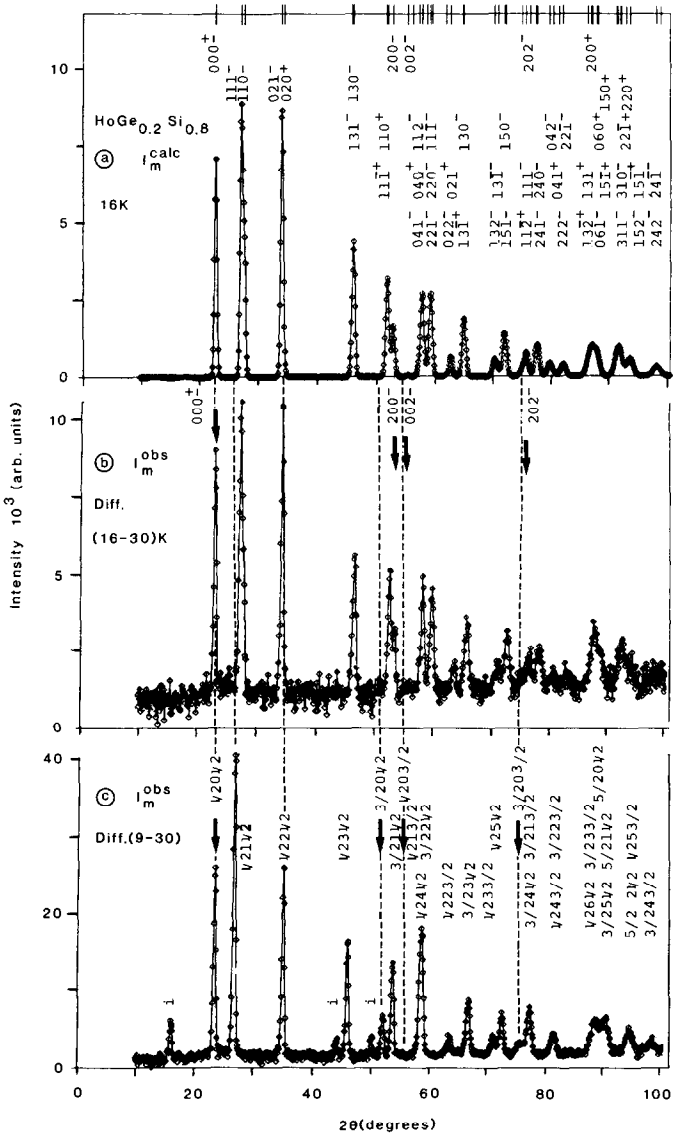

FIG. 6. Magnetic neutron diffraction patterns of $HoGe_{0.2}Si_{0.8}$ at 16 and 4.2 K. (a) Calculated profile at 16 K of the incommensurate phase [$\mathbf{k}$ = 0.459, 0., 0.511]. Only magnetic reflections were considered. The difference diagrams obtained by substracting the data found in the corresponding paramagnetic states are shown in the middle part (b) and at the bottom part (c) of the figure.

The scattering intensity of a magnetic satellite reflection ($H \pm k$) for the sinus modulation (*11*) is proportional to

$$\sigma_{H\pm k} = \frac{\sin^2\omega}{4}\left[\left(\frac{\hat{\mathbf{e}}^2}{2mc^2}\right)\sum_V \mu_V^0 f_v(\mathbf{H} \pm \mathbf{k}) \exp i(2\pi\, \mathbf{H}\cdot\mathbf{r}_\nu \mp \phi_\nu)\right]^2. \quad (2)$$

μ_V^0 is the moment value (amplitude), ω is the angle between the direction of the varying moment component and the scattering vector $\hat{\mathbf{e}}$, and ϕ_V ($V = 1, 4$) is the phase angle of the moments within the chemical cell. The calculation of the magnetic intensities at 16 K was carried out using the scale factor and the refined parameters that were derived from the nuclear intensity data of $HoGe_{0.2}Si_{0.8}$ obtained at 30 K. The intensities of this latter diagram (measured under the same conditions) have been substracted from the 16.5 K data in order to provide a greater number of resolved observed magnetic peaks. The corresponding difference diagram is shown in Fig. 6b.

The best agreement between the observed and the calculated intensities (R_m = 7%) was achieved for a moment value of 6.1 μ_B and for a moment direction in which all atomic moments are lying in the plane (x 0 z) and are oriented almost parallel to the c-axis ($\varphi_z = 5(1)°$). The relation between the magnetic intensities and the moment angle φ_z is shown in Fig. 7. The intensity ratio of three resolved reflections to the zero-point satellite shows a rather steep increase when the angle φ_z is increased from 0 to 30°. The experimental values correspond to the moment angle of 5(1)° which is close to the value observed for the lock-in structure (7°). It is noteworthy that the incommensurate structure bears a similarity to the canted model (left) of Fig. 8, which has a higher symmetry. Furthermore, it would not be possible to reproduce the observed intensities on the basis of the phase relations of the collinear model (right) (having three atoms parallel and one atom antiparallel within the chemical cell).

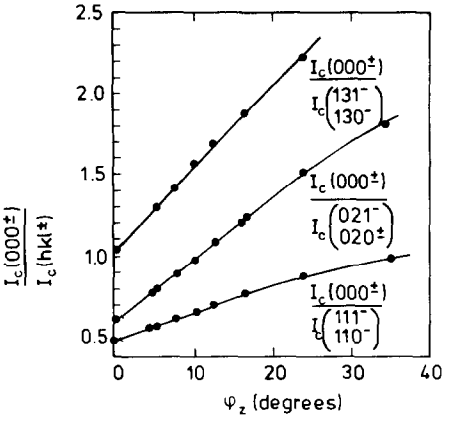

FIG. 7. The ratio of the intensity of the three magnetic satellites to the intensity of the zero-point satellite as a function of the angle ϕ_z between the moment direction in the incommensurate structure and the c-axis.

Inspite of the similarity between the canted structure and the lock-in structure the intensity calculation cannot be procured by the same formula since the structures are of a different nature (*5*) and are described by the wave vectors $\mathbf{k}_9 = [\frac{1}{2}\ 0\ \frac{1}{2}]$ and $\mathbf{k}_2 = [q_x\ 0\ q_z]$ in the notation of Ref. (*12*). The star of the wave vectors has two and four arms, respectively. The corresponding order parameters have the dimensions 4. The two wave vectors correspond to different irreducible representations. The irreducible representation associated with the wave vector $\mathbf{k}_2$ is one dimensional, as expected for a sinus modulation. The transition from one structure to the other, as already mentioned, is most probably of first order. Therefore it is associated with a discontinuous change of the order parameter and depends on both the temperature and the composition.

The intensity calculations of the incommensurate structure were carried out for all equivalent reflections and for one arm of the wave vector star and added up. The

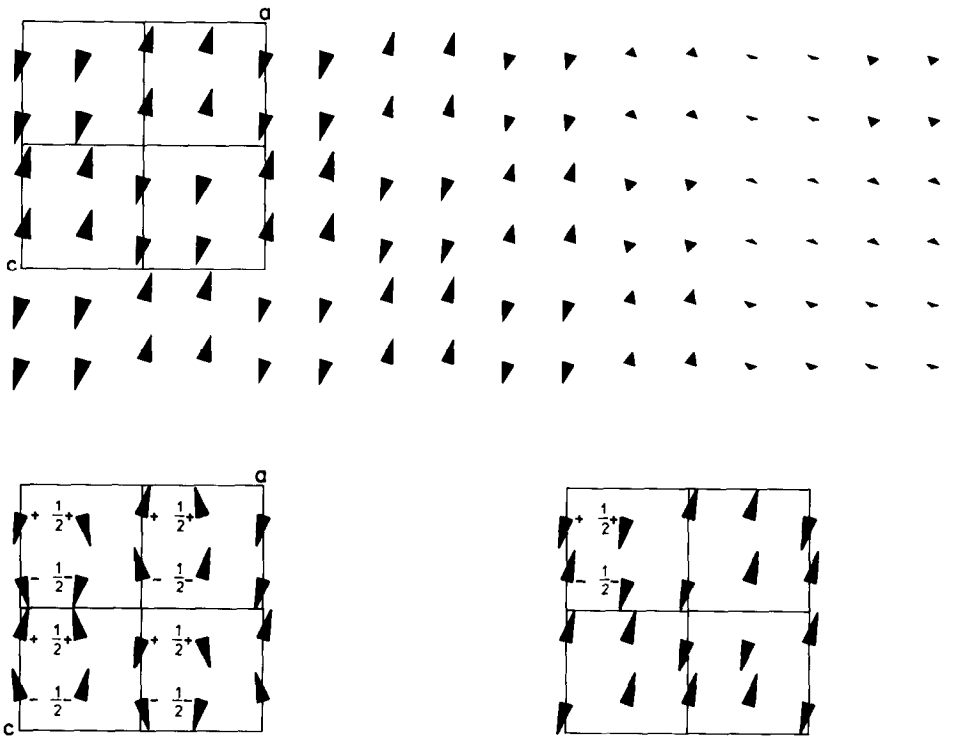

FIG. 8. Schematic representation of the incommensurate magnetic structure (only magnetic atoms are shown) proposed for the high-temperature magnetic phase of $HoGe_{0.2}Si_{0.8}$ ($T_{ic} \leq T \leq T_N$). In the bottom part of the figure the incommensurate structure is compared with two types of structures proposed for the low-temperature commensurate phase. All figures are projections onto the ($x0z$) plane.

corresponding intensities are listed in Table III and compared with the results obtained for the commensurate structure at 4.2 K. The splitting of all satellites observed can be derived from the comparison of the corresponding 2θ values at the two temperatures. The profile calculated for the whole 2θ region considered is displayed in Fig. 6a and shows good agreement with the experimental data.

The incommensurate model shown in Fig. 8 corresponds to a sinusoidal moment modulation in the direction of the wave vector [0.459, 0., 0.511]. The moment is polarized in the [$\bar{1}$ 0 10] direction which is 5.2° off the z-axis. The phase difference between translational equivalent atoms is $2\pi q_x = 165.2°$ along x and $2\pi q_z = 183.9°$ along the z direction, compared to 180° in the lock-in structure. The moment value reduces almost to zero after 6 cells in the x direction and readopts its original value after 12 cells. The modulation in the z direction is rather smooth and about 23 cells are needed for the moment to disappear, and 46 cells are required to reach its original value. One may figure that at T_{ic} half of the moments of the canted model may turn by almost 10° and align themselves parallel within the cell when the wave vector jumps to the incommensurate value and the lattice loses its translational periodicity in two directions. The change of the wave vector length in the remaining

temperature interval up to T_N is less pronounced, as will be shown in the next section.

2.4. *The Temperature Dependence of the Wave Vector* $[q_x\ 0\ q_z]$ *in* $HoGe_{1-x}Si_x$

Difference diagrams obtained from neutron diagrams pertaining to the ordered (commensurate or incommensurate) state after subtraction of the neutron intensities pertaining to the paramagnetic state may provide useful information when analyzing data obtained by powder diffraction. It is extremely helpful, in particular, when indexing incommensurate structures for which the wave vector may have a general position in space. This procedure (5) is applied in the data analysis of $HoGe_{0.2}Si_{0.8}$ for the temperatures 4.2 K (lock-in structure), 16.3 K (incommensurate structure), and 30 K (paramagnetic state). One may recognize in Figs. 6b and 6c that, apart from the zero-point satellite $[\frac{1}{2}\ 0\ \frac{1}{2}]$ at $2\theta = 23.4°$, three additional $[h/2\ 0\ l/2]$ reflections occur, the locations of which are indicated by arrows. However, only the $[\frac{3}{2}\ 0\ \frac{1}{2}]$ reflection (at $2\theta = 51.95°$) is well resolved. This latter reflection together with the $[\frac{1}{2}\ 0\ \frac{1}{2}]$ reflection has been used for deriving the q_x and q_z wave vector components. A q_y modulation has been ruled out from the fact that the zero-point satellite moves to smaller angles.

The $[\frac{3}{2}\ 0\ \frac{1}{2}]$ reflection, like all the other $[h/2\ 0\ l/2]$ reflections, shows a shift in 2θ but does not split. In contrast to the (000^+) satellite the reflection $[\frac{3}{2}\ 0\ \frac{1}{2}]$ moves toward higher angles above T_{ic}. The shift in 2θ at a temperature just 1 K above the transition point is almost 2° ($2\theta = 53.59°$, see Fig. 6b). The $[\frac{3}{2}\ 0\ \frac{1}{2}]$ reflection corresponds to the (200^-) satellite as shown in (5). After inserting the experimental $\sin^2\theta$ values observed at 16.5 K for the (000^+) and (200^-) satellites in formula (1) we obtain a system of two equations which may be used for deriving q_x and q_z. The first estimates of the values [0.45, 0., 0.51] were used to index the 16.5 K data over a large 2θ region. Subsequently the refined value [0.459, 0., 0.511] was obtained. The 2θ values calculated show a satisfactory agreement, up $2\theta = 100°$, with the 2θ values observed, as is seen in Table III.

The temperature dependence of the wave vector components for three compounds is shown in Fig. 9. The q_z values, which are related to the splitting of the $[\frac{1}{2}\ 1\ \frac{1}{2}]$ reflection by the expression (5)

$$q_z = \frac{2c^2}{\lambda^2}(\sin^2\theta_{110^-} - \sin^2\theta_{111^-}) + 0.5, \quad (3)$$

were calculated for all temperatures up to T_N. In a similar manner the values of q_x were derived from the 2θ values of the zero-point satellite:

$$q_x = a\left[\frac{4\sin^2\theta_{000\pm}}{\lambda^2} - \frac{q_z^2}{c^2}\right]^{1/2}. \quad (4)$$

The germanium-rich compound $x = 0.2$, which remains incommensurate down to 1.2 K, shows a linear decrease and increase with increasing temperature of the q_x and the q_z components, respectively. From Fig. 9 it can be deduced that the lock-in structure may arise by a jump of the wave vector

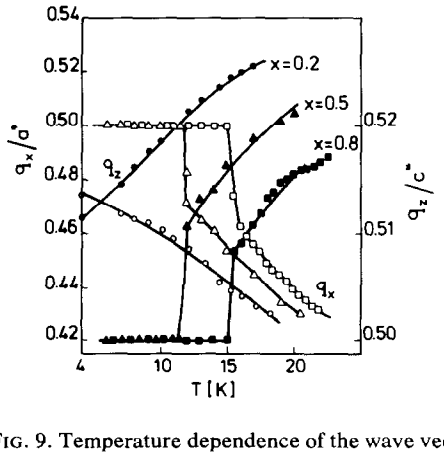

FIG. 9. Temperature dependence of the wave vector components q_x (open symbols) and q_z (filled symbols) for various compositions of the $HoGe_{1-x}Si_x$ system.

below 1.2 K and not by a continuous wave vector change (a linear extrapolation would correspond to a lock-in temperature of −6 K). The q_z values of this compound are better approximated by the multi-Gauss fitting procedure than those for which $x > 0.2$, since the unfolding of this satellite is already completed at 4.2 K. Close to T_N = 19 K the wave vector of this compound shows the largest deviation from the lock-in value [½ 0 ½] occurring in this system [0.43, 0, 0.527]. The incommensurate region becomes reduced with increasing silicon content. For the pure HoSi compound, which is not included in Fig. 9, the incommensurate region is only 7°. It is difficult from the accuracy of our data to comment on the wave vector values for temperatures just above T_{ic}. The common characteristic of the magnetic phase transition observed for all compounds is that the wave vector changes discontinuously to an incommensurate value for which $q_x < \frac{1}{2}$ and $q_z > \frac{1}{2}$. It cannot be excluded that the incommensurate value at each T_{ic} is the same for all compositions since above T_{ic} the wave vector components for all compositions vary linearly with temperature, the corresponding curves having almost the same slope. The wave vector length changes quite smoothly in the region between T_{ic} and T_N along a line that makes an angle of 13° with the a-axis, while the moment direction does not change and remains close to the c direction.

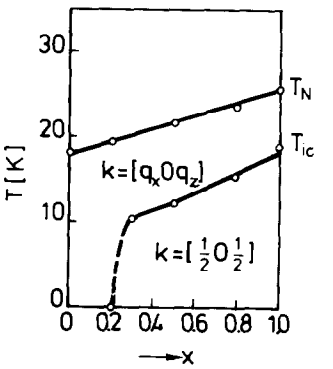

FIG. 10. Magnetic phase diagram of the $HoGe_{1-x}Si_x$ system.

3. Concluding Remarks

The magnetic phase diagram of the system $HoGe_{1-x}Si_x$, shown in Fig. 10, comprises three distinct regions. The paramagnetic phase is stable at high temperatures. At temperatures below T_N there is a region where the magnetic ordering leads to an incommensurate structure. At still lower temperatures it passes into a region where the magnetic structure is commensurate. However, this latter region is not found in the Ge-rich corner. Here the incommensurate structure extends to all temperatures considered by us in this investigation. It is interesting to compare the phase diagram for $HoGe_{1-x}Si_x$ with the phase diagram obtained by us for $TbGe_{1-x}Si_x$ (5). At the Si-rich end (disregarding the crystallographic structure change) both phase diagrams bear the same features, decreasing temperature leading from the paramagnetic regime first into the incommensurate regime and eventually reaching the commensurate regime where magnetic structures of the type [½ 0 ½] are stable. The phase diagram of the $TbGe_{1-x}Si_x$ system differs from the Ho $Ge_{1-x}Si_x$ one insofar as the regime of the [½ 0 ½] structure extends to all concentrations. Moreover, the regime of the incommensurate phase extends to concentrations above $x \approx 0.6$. A commensurate phase of the type [0 0 ½] is found instead of this incommensurate phase for Si concentrations lower than $x \approx 0.6$. In an attempt to trace the origin of the magnetic phase transformations occurring below T_N one might wonder whether the interatomic distances and hence the lattice constants play an important role. In

view of the chemical similarity between Ge and Si it seems not unlikely that the concentration-induced change from the commensurate [0 0 ½] type of structure to the incommensurate [q_x 0 q_z] type of structure at intermediate temperatures in the $TbGe_{1-x}Si_x$ system is to be associated with the decreasing lattice constants with increasing x. If the lattice constants found for $TbGe_{0.4}Si_{0.6}$ are considered as marking the limit for the occurrence of the [0 0 ½] type one finds from the lattice constants of the $HoGe_{1-x}Si_x$ compounds that the situation in the latter system should correspond to a situation found in the Si-rich side of the $TbGe_{1-x}Si_x$ system. In other words, for the lattice constants found in the $HoGe_{1-x}Si_x$ system one expects only three regions to be present in the phase diagram, comprising the paramagnetic region, the incommensurate region ($\mathbf{k} = [q_x\ 0\ q_z]$), and the commensurate region ($\mathbf{k} = [\frac{1}{2}\ 0\ \frac{1}{2}]$). The agreement with the phase diagram actually observed for $HoGe_{1-x}Si_x$ is gratifying. However, some preliminary data obtained for the compound DyGe indicate that this approach might be an oversimplification. More experimental information is required to obtain a better understanding of the development of the magnetic phase diagrams in the various $RGe_{1-x}Si_x$ pseudobinary systems. An extension of our experiments in this direction is planned in the near future.

Acknowledgments

The authors thank Professor P. Tolédano, Dr. P. Fischer, and Dr. B. Hälg for fruitful discussions and the Laboratorium für Neutronenstreuung of the ETH Zürich for technical support.

References

1. D. Hohnke and E. Parthé, *Acta Crystallogr.* **20,** 572 (1966).
2. K. H. J. Buschow and J. F. Fast, *Phys. Status Solidi* **16,** 467 (1966).
3. Nguyen Van Nhung, A. Barlet, and J. Laforest, *J. Phys. Coll. Cl Suppl.* **32**(2-3), cl-1133 (1971).
4. P. Schobinger-Papamantellos and K. H. J. Buschow, *J. Magn. Magn. Mat.* **44,** 149 (1984).
5. P. Schobinger-Papamantellos and K. H. J. Buschow, (a) *J. Magn. Magn. Mat.* **62,** 15 (1986) and (b) submitted for publication.
6. H. M. Rietveld, "RCN Rep. 104," Petten, The Netherlands (1970).
7. L. Koester and A. Yelon, "Summary of Low Energy Neutron Scattering Lengths and Cross Sections" (1983). (Data of the Neutron Diffraction Commission, available from Dr. G. Bergsma, ECN, Postbus 1, 1755 ZG Petten, The Netherlands.)
8. A. J. Freeman and J. P. Desclaux, *J. Magn. Magn. Mat.* **12,** 11 (1979).
9. B. A. Koptsik, "Shubnikov Groups," Moscow Univ. Press, Moscow (1966).
10. V. N. Nguyen, F. Tchéou, and Rossat-Mignot, *J. Phys.* **45,** 163 (1984).
11. B. van Laar, "RCN-92 Report," Petten, The Netherlands (1968).
12. O. V. Kovalev, "Irreducible Representations of the Space Groups," Gordon & Breach, New York (1965).